Finite Elements in Analysis and Design 89 (2014) 8–18

Contents lists available at ScienceDirect

Finite Elements in Analysis and Design

journal homepage: www.elsevier.com/locate/finel

Numerical modeling of friction stir welded aluminum joints under high rate loading

Colin McAuliffe [a], Ryan Karkkainen [b,*], Chian Yen [c], Haim Waisman [a]

[a] Department of Civil Engineering & Engineering Mechanics, Columbia University, New York, NY 10027, United States
[b] Department of Mechanical and Aerospace Engineering, University of Miami, Coral Gables, FL 33146, United States
[c] U.S. Army Research Laboratory Materials and Manufacturing Science Division Aberdeen Proving Ground, MD 21005, United States

ARTICLE INFO

Article history:
Received 10 October 2013
Received in revised form
23 April 2014
Accepted 29 April 2014
Available online 20 June 2014

Keywords:
Computational mechanics
Shear band
Friction stir weld

ABSTRACT

Prediction of shear band formation and other strain localization processes presents many computational challenges that must be overcome to enable dynamic failure prediction and material design of ductile material systems. The current work presents a finite element based computational framework accounting for this critical deformation process, as applied to a detailed investigation of friction stir welded (FSW) aluminum joints. A stir welded joint has several zones, each with distinct microstructural characteristics and material properties. For applications in Army land vehicles, which may be subject to under-body blast, an understanding of the energy absorption capability of these joints is needed. Thus material inhomogeneity, dynamic loading, and detailed understanding of small scale failure processes must all be accounted for to accurately model FSW material behavior. In this study, an implicit nonlinear consistent (INC) or monolithic solution technique is used to predict shear band formation and estimate the energy absorption and failure strain of a stir welded aluminum joint. It has been shown that failure initiating at material interface regions can be predicted, and furthermore that abrupt material property gradients predominantly contribute to FSW joint failure.

1. Introduction

High strength lightweight aluminum alloys offer potential advantages as replacements for traditional steels in many Army vehicles in terms of weight specific mechanical properties. Unibody chassis construction, as opposed to body on frame construction, is being pursued to lend enhanced rigidity to maintain structural integrity during potential under-body blast events. Since unibody construction requires the elimination of bolted joints, weldability of the chassis material is crucial. Alloys from the aluminum 2XXX and 5XXX series are notoriously difficult to weld with conventional techniques, but can be joined with Friction Stir Welding (FSW) [1].

FSW is a solid state joining process, which has recently been shown to be capable of producing joints in aluminum up to 76.2 mm thick [2,3]. The FSW tool consists mainly of a shank, shoulder, and pin (shown in Fig. 1), which rotate as they advance, stirring the material together. Significant inelastic deformation, heat production, and dynamic recrystallization occur during this process, which results in the formation of several zones with distinct microstructure and material properties [4–9].

Fig. 2 shows a cross-section of a typical FSW joint, in this case 2139 Aluminum, which illustrates the nature of these distinct material zones. The material zone most immediately surrounding the high-torque tool pin, inserted between the welded plates, is characterized by an upper and a lower weld nugget. The upper and lower weld nuggets are zones B and A, respectively, in Fig. 2. This comes as a direct influence of the tool pin on the material grain structure as well as the thermal properties of the material and recrystallization processes. The tool shoulder creates a great deal of friction in contact with the plate surface during the FSW process which generates an inordinate amount of heat in comparison to the bottom of the plate [10]. The difference in thermal inputs and boundary conditions thus creates a through thickness variation in recrystallization and grain growth which leads to the distinct lower and upper weld nuggets, marked as zones A and B, respectively in Fig. 2. Note that for thin welds there is no readily discernible difference between the upper and lower nuggets; however, welds of, at least 2 cm thick are of the greatest interest for Army land vehicle applications. At this thickness there is a clear distinction between the upper and lower nuggets, as shown in [11,12]; just outside of the weld nugget, zone C in Fig. 2, is a third material zone which is still subject to both the mechanical and the

* Corresponding author.
E-mail address: r.karkkainen@miami.edu (R. Karkkainen).

http://dx.doi.org/10.1016/j.finel.2014.04.012
0168-874X/

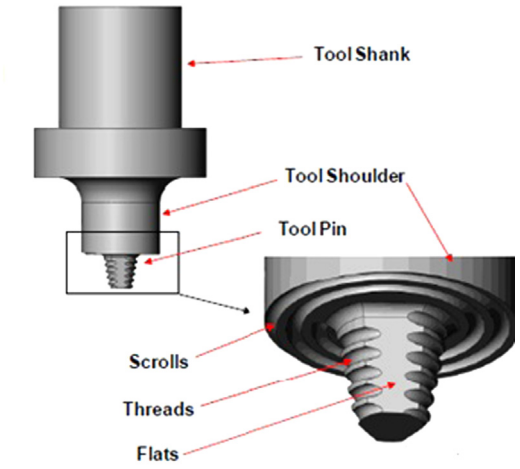

Fig. 1. FSW tool. The tool shoulder is butted against the workpiece and the tool is rotated as it advances. This process mechanically stirs the workpiece metals together at elevated temperature, but without melting.

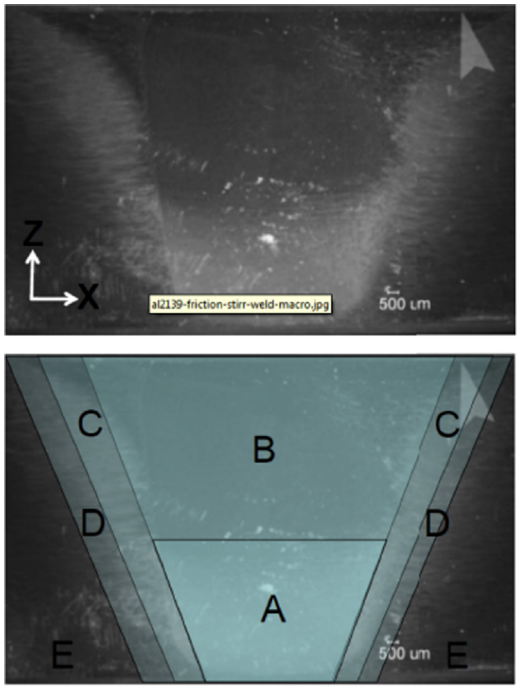

Fig. 2. FSW cross section for 2139 Aluminum. The labeled areas correspond to different weld zones which have distinct microstructural and mechanical properties. Zone A is the lower weld nugget, B the upper weld nugget, C the thermo-mechanical affected zone, and D the thermal affected zone.

thermal influence of the FSW stirring pin. Further from the tool is a fourth material zone, too distant to be influenced by mechanical stirring, but still subject to thermal microstructural effects as heat is conducted away from the FSW joint during processing. This is known as the thermal affected zone and is marked by zone D in Fig. 2. The importance of accounting for these variations must be noted, and they will play a significant role in the simulations below. Computational modeling of the FSW process, aimed at numerically predicting the FSW joint zones, has been carried out by [13–15] on joints 6.35 mm thick and by [16–18] on joint 7 mm thick. Additional computational studies by [19,20] sought to determine how the FSW process parameters such as tool advancement speed affect the final weld. The studies cited above used either a Lagrangian or an Arbitrary Lagrangian Eulerian (ALE) type of numerical formulation with adaptive remeshing. However, Eulerian formulations are also available [21].

In this study, we numerically model high rate loading of a small cross section of a stir welded joint. The goal is to develop a predictive capacity for energy absorption and failure of FSW joints in dynamic loading, as well as to gain an understanding of the relationship between an FSW joint microstructure and the resulting energy absorption capability and failure strain. It is found that the presence of the abruptly changing material zones leads to significantly reduced energy absorption capacity of the FSW joint in comparison to two benchmark tests with uniform material properties. The benchmarks used the material properties of the unaffected material and the lower nugget, the nominally weakest of the weld zones. This suggests that weld capacity can be improved by altering the FSW process parameters such that the final weld contains more smoothly varying zones.

2. Shear band model and numerical implementation

Preliminary formulations showing reliable, mesh insensitive results for shear bands have been studied at small strains in [22]. The governing equations considering small strain deformation are as follows:

$$\rho\ddot{u}_i = \sigma_{ij,j} \tag{1}$$

$$\dot{\sigma}_{ij} = C^{elas}_{ijkl}\left(d_{kl} - \frac{3}{2\overline{\sigma}}g(\overline{\sigma},T,\overline{\gamma}^p)s_{kl} - \alpha\dot{T}\delta_{kl}\right) \tag{2}$$

$$\dot{\overline{\gamma}}^p = g(\overline{\sigma},T,\overline{\gamma}^p) \tag{3}$$

$$\rho c\dot{T} = \kappa T_{,jj} + \chi\overline{\sigma}g(\overline{\sigma},T,\overline{\gamma}^p) \tag{4}$$

where the unknown fields are the displacement u_i, the stress σ_{ij}, the temperature T, and the equivalent plastic strain $\overline{\gamma}^p$. The material parameters are the density ρ, the elastic modulus C^{elas}_{ijkl}, the thermal expansion constant α, the specific heat c, and the thermal conductivity κ. The function g is the inelastic constitutive law, which hardens with increasing plastic strain and strain rate, and softens with temperature. Note that an additive split of the deformation rate into elastic, inelastic and thermal parts has been used. A J2 plasticity model has been employed; the inelastic constitutive relation thus depends on the Von Mises stress $\overline{\sigma}$ such that

$$\overline{\sigma} = \sqrt{\tfrac{3}{2}s_{ij}s_{ij}} \tag{5}$$

where the deviatoric stress s_{ij} is defined as

$$s_{ij} = \sigma_{ij} - \frac{1}{3}\sigma_{kk}\delta_{ij} \tag{6}$$

Heat is produced in proportion to the inelastic work rate $\sigma_{ij}d^p_{ij} = \overline{\sigma}g$. The so-called Taylor Quinney fraction χ determines how much inelastic work is converted to heat and is typically chosen as a constant in the range of 0.85–0.95 for most computations [23].

The PDE model was discretized in a mixed finite element framework with a monolithic nonlinear solution scheme, where all four of the unknown fields above are updated simultaneously. The discretization and time marching scheme can be found in [22]. We define the weak form residual of the system as $\mathbf{F}[\mathbf{p}]$, where $\mathbf{p} = [\mathbf{u}\ \boldsymbol{\sigma}\ T\ \gamma_p]^T$ is the solution field. Here, $\mathbf{u}$ is the displacement, $\boldsymbol{\sigma}$ the stress, T the temperature and γ_p the equivalent plastic strain.

It is important to note that at each time step, Newton iterations are performed until convergence, in contrast to split solution schemes [24–27], where the solution is updated with one